Diamond nucleation density as a function of ion-bombardment energy in electron cyclotron resonance plasma

Yutaka Kouzuma, Kungen Teii,* Kiichiro Uchino, and Katsunori Muraoka
Department of Applied Science for Electronics and Materials, Interdisciplinary Graduate School of Engineering Sciences, Kyushu University, Kasuga, Fukuoka 816-8580, Japan
(Received 10 March 2003; published 7 August 2003)

A low-pressure study on diamond nucleation on mirror-polished Si(100) wafers using defined ion-bombardment energy is presented. The substrate was negatively biased to several tens of V in an electron cyclotron resonance methane-hydrogen plasma at 1×10^{-3} Torr for nucleation, and then exposed to a typical hot-filament system at 40 Torr for subsequent growth. The nucleation density counted after the growth was enhanced up to $\sim10^{8}$ cm^{-2} for a narrow bias-voltage range of -20–-50 V in the initial nucleation treatment. The threshold and optimum ion energies for the nucleation enhancement were found to be 20–30 eV and around 50 eV, respectively, just above the threshold for shallow ion implantation. Cross-sectional transmission electron microscopy and selected-area electron diffraction for the deposits after the nucleation treatment revealed that diamond crystallites with sizes smaller than a few tens of nm were embedded in a matrix of amorphous carbon. The nucleation density as a function of ion energy was compared with the fractional increase in carbon sp^3 bonding caused by subplantation. The results confirm the nucleation pathway through the ion-induced densification beneath a surface, which is largely different from the conventional condensation of adsorbed species on a surface.

DOI: 10.1103/PhysRevB.68.064104 PACS number(s): 81.05.Uw, 81.07.Bc, 52.77.Dq, 68.55.Jk

I. INTRODUCTION

Vapor-phase deposition of high-quality and oriented diamond films on low-cost foreign substrates like Si wafers has been pursued to apply diamond films to high-performance electronic devices. The major goal is the heteroepitaxial growth as in the case of other semiconductor films now in practical use. For this purpose, a primary difficulty lies in the nucleation on such foreign substrates without unfavorable mechanical pretreatments. This has mainly been ascribed to the large difference in the lattice constants and the surface free energies for diamond and underlying substrates. Numerous trials have been made to form an appropriate interface layer, which allows the system to approach the wetting condition, a criterion for nucleation with no potential barrier. These include carburization, carbon coating, ion implantation, and positive or negative substrate biasing.[1] In a past decade, the electrical bias effects have been intensively investigated in conjunction with the bias-enhanced nucleation (BEN) technique which can achieve a high nucleation density up to 10^{9}–10^{10} cm^{-2}.[2] In the BEN technique, a negative direct-current (dc) bias up to a few hundreds of V is applied to a substrate at moderate pressures of a few tens of Torr. Energetic ion-bombardment that *will* be induced by a large potential drop over the substrate surface has been considered as the principal driving force for the nucleation enhancement.[3–5] However, no decisive evidence for the ion-induced nucleation has so far been presented because of the complicated gas-phase and surface processes in collisional high-pressure conditions.

As a matter of course, low-pressure conditions are desired to simplify the definition and control of incident ion energy and flux. The number of low pressure studies on diamond deposition is very small because low radical fluxes, high ion energies, and high ion-to-neutral flux ratios specific to low pressures are believed to be unfavorable for diamond deposition, where static conditions not far from thermodynamic equilibrium are usually preferred. In fact, a previous study below 20 mTorr has showed that faceted diamond can only be grown with an ion-bombardment energy as low as a few eV.[6] In particular, the nucleation at such pressures is very difficult, even with mechanical pretreatments, since the fluxes of carbonaceous radicals required for a high degree of local supersaturation inevitably decrease. Some exceptional studies have revealed that small crystallites with diamond structure embedded in amorphous matrix can be prepared under ion bombardment with high kinetic energies of tens to hundreds of eV.[7–11] This energy level is much higher than zero to several eV for normal diamond deposition, and is often related to shallow ion implantation into a subsurface of a film, typical for diamond-like carbon film deposition.[12] However, the nucleation mechanism has not thoroughly been investigated with respect to the variation of ion energies. It is necessary to obtain mechanistic insights into such an unusual nucleation process with well-defined ion energies, preferably to develop a superior pathway to the BEN.

In this study, the effect of ion-bombardment on diamond nucleation on Si in electron cyclotron resonance (ECR) plasma is presented. In particular, the relationship between the ion-bombardment energy and the nucleation density is systematically studied. A mirror-polished Si(100) substrate is negatively biased to several tens of V in an ECR CH_4-H_2 plasma at 1 mTorr for nucleation, and then exposed to a typical hot-filament (HF) chemical-vapor deposition (CVD) system at 40 Torr for subsequent growth so as to readily examine the nucleation density. Here we selected an ECR plasma source because it could provide a high ion flux even at a low ion energy, superior to an ion-beam source. It will be shown that nanocrystalline diamond can be formed at rela-

 ©2003 The American Physical Society

TABLE I. Summary of deposition conditions.

	Surface cleaning (ECR plasma)	Nucleation (ECR plasma)	Growth (HF)
Pressure (Torr)	5×10^{-3}	1×10^{-3}	40
MW power/Filament temperature (W or °C)	500	500	2150
H_2 concentration (vol.%)	100	50	99.2
CH_4 concentration (vol. %)	0	50	0.8
Total flow rate (sccm)	20	20	200
Substrate temperature (°C)	~450 to 700[a]	700	1000
Substrate dc bias (V)	floating	0 to −100	floating
Duration (min)	10	60	90

[a]The temperature was elevated from ~450 to 700 °C during this cleaning process.

tively low ion energies of 20–50 eV, just above the threshold for shallow ion implantation. The results confirm the nucleation pathway beneath a film surface caused by energetic ion bombardment.

II. EXPERIMENT

An ECR plasma reactor consisted of a magnetron head, a waveguide, a grounded chamber, and two electromagnetic coils. The microwave (MW) power of 500 W at 2.45 GHz was supplied through a quartz vacuum window located on the top of the chamber. A divergent magnetic field was produced by the electromagnetic coils, and then the ECR point at 875 G was set at 150 mm above the substrate. Prior to deposition, an *n*-type Si(100) wafer was cleaned with acetone in an ultrasonic generator, dipped in 1.5% hydrofluoric solution diluted in deionized water for 30 s to remove native oxide, and rinsed in deionized water. The substrate was then mounted on a stainless steel holder equipped with a Mo electrode and a Ta wire heater. The substrate temperature (T_s) was monitored using a thermocouple attached to the backside of the substrate. The experimental conditions are given in Table I. The experiments included three steps: (1) initial exposure to an ECR H_2 plasma at 5 mTorr for *in-situ* cleaning of the substrate surface, (2) nucleation treatment in an ECR 50% CH_4 − 50% H_2 plasma at 1 mTorr, and (3) subsequent growth of the already formed nuclei in a mixture of 0.8% CH_4–99.2% H_2 by HFCVD at 40 Torr. Note that a dc bias (V_b) was applied to the substrate during the nucleation treatment [step (2)]. The plasma potential (V_p) at about 10 mm above the substrate was measured by the emissive probe method using a Ta filament tip connected with an isolation transformer, a volt slider, and an oscilloscope, to determine the sheath potential, $V_{sh}=V_p-V_b$. The surface morphology of the deposits was examined by field-emission scanning electron microscopy (SEM). The structure and the crystallinity were examined by x-ray diffraction (XRD) measurement with CuKα radiation (1.54 Å) and micro-Raman spectroscopy with Ar^+ laser excitation (514.5 nm). Transmission electron microscopy (TEM) and selected-area electron diffraction (SAED) were used to probe cross-sectional microstructures at the deposit-Si interface. A focal area of the electron beam for SAED was about 200 nm. The TEM sample was prepared by Ar^+ ion-beam thinning.

III. RESULTS

The influence of V_b on V_p in the ECR 50% CH_4 – 50% H_2 plasma is shown in Fig. 1. The experimental error of V_p was estimated to be within ±1 V. For positive V_b, V_p increased in proportion to V_b, thus V_{sh} remained constant at around 10 V. In contrast, for negative V_b, V_p decreased from 10 to 0 V for V_b from 0 to −30 V and remained constant at around 0 V for V_b exceeding −30 V. A possible explanation for the variation of V_p with V_b is given based on the current balance between the substrate and the chamber wall.[13] This result confirms that V_{sh} can be varied over a wide voltage range by applying negative V_b. An ion collision probability in the sheath is characterized by the ratio of a sheath thickness to an ion mean-free path. The thickness of a static and collisionless sheath (d_s) is given by

$$d_s \approx \lambda_D \left(\frac{eV_{sh}}{k_B T_e} \right)^{3/4}, \tag{1}$$

where λ_D is the Debye length, e the elementary electron charge, k_B the Boltzmann constant, and T_e the electron temperature. Substitution of $\lambda_D = 0.08$ mm and $T_e = 3.5$ eV measured in an ECR H_2 plasma using a Langmuir probe into Eq. (1) yields d_s in the range of 0.2 to 1.0 mm for V_{sh} of 10 to 100 V. An ion mean-free path (λ_i) at 1 mTorr and 300 K is estimated to be ~10 mm, almost independent of ion energies of interest, for symmetric, resonant charge-exchange collisions with neutrals in a N_2^+-N_2 system.[14] This indicates that the ion collision probability (d_s/λ_i) in the present experiments is much smaller than unity for any V_{sh}. The incoming ions obtain a whole V_{sh} during the sheath transit, thus V_{sh} could correspond to the mean ion energy. In fact, under similar plasma conditions, a comparison of ion energies measured by a probe and an ion energy analyzer revealed that V_{sh} coincided with the mean ion energy within an error of 0.5 eV at pressures below 10 mTorr.[15]

The number density of crystal islands after the growth in the HF system could be greatly enhanced by the nucleation treatment with high CH_4 concentrations, high T_s, and negative V_b. Typical SEM images and Raman spectra for the deposits after the nucleation treatment with $V_b = -30, -50$, and −70 V and the subsequent growth are shown in Figs. 2(a)–2(c) and Fig. 2(d), respectively. For a small range of V_b

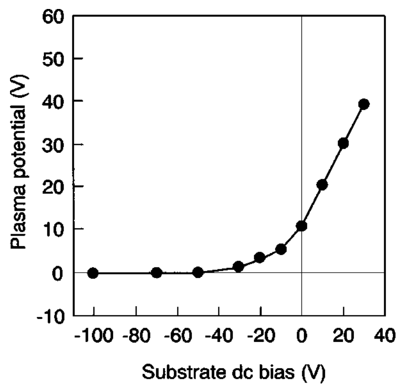

FIG. 1. Plasma potential in the ECR 50% CH_4 − 50% H_2 plasma at 1 mTorr as a function of substrate bias voltage.

between −20 and −50 V, we could enhance the resultant nucleation density up to $\sim 10^8$ cm^{-2}. This is the same order of magnitude as reported in a similar low-pressure study by ion-beam deposition.[11] For $V_b = -30$ and −50 V [Figs. 2(a) and 2(b)], faceted diamond crystals with sizes smaller than 2 μm are grown randomly and dispersed uniformly on the whole substrate surface. For $V_b = -70$ V [Fig. 2(c)], the crystals are spherical without facets and their number density is very small. The Raman spectra [Fig. 2(d)] corresponding to Figs. 2(a)–2(c) exhibit signatures of cubic diamond at around 1332 cm^{-1}, together with the broad *G* line peaks at 1580–1600 cm^{-1} from amorphous graphitic carbon. The crystallinity for $V_b = -50$ V is the highest because the full width at half maximum (FWHM) of the diamond peak is the smallest (~ 9 cm^{-1}). It should be noted that the crystal size, morphology, and crystallinity in addition to the nucleation density after the growth under an equivalent HF environment depend on V_b and hence V_{sh} during the initial exposure of the substrate to the ECR plasma. This indicates that the nature of deposits after the growth indirectly reflects that after the nucleation treatment.

The relationship between the resultant nucleation density after the growth and the negative V_b in the initial nucleation

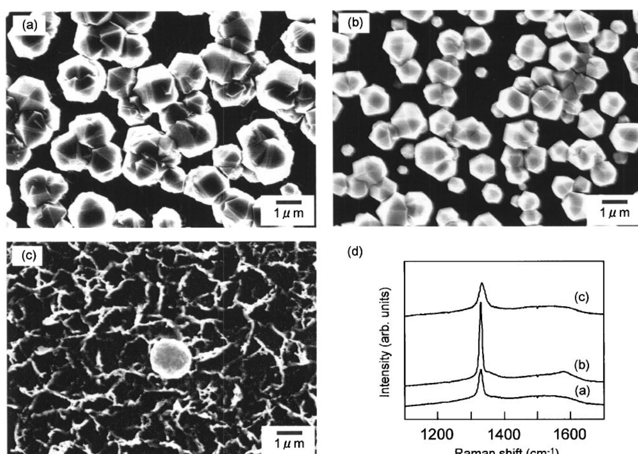

FIG. 2. SEM images of diamond crystals after the nucleation treatment and subsequent growth with (a) $V_b = -30$ V, (b) $V_b = -50$ V, and (c) $V_b = -70$ V. (d) Raman spectra corresponding to the deposits shown in (a)–(c).

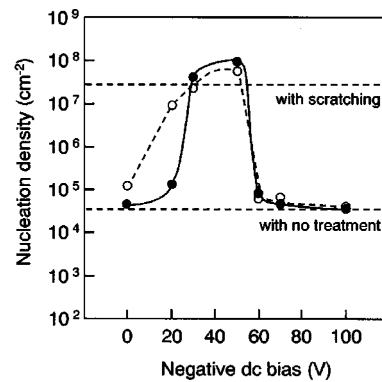

FIG. 3. Diamond nucleation density after the nucleation treatment and subsequent growth as a function of substrate bias voltage. Two sets of data obtained by the different growth methods, HFCVD (filled circles) and MW plasma CVD (open circles, from Ref. 16), are plotted. Two horizontal lines are the densities with scratching and no treatment, respectively. The solid and dashed curves are guides to the eyes.

treatment is shown in Fig. 3. Another set of data obtained by the growth in a typical MW plasma is cited from our previous study[16] and plotted for comparison. The two sets of data for the HF system and the MW plasma are in reasonable agreement, suggesting that the results are highly reproducible. Besides, the identical nucleation density, crystal morphology, and crystallinity by the two different growth methods also indicate that the nature of deposits after the growth depends mainly upon that after the nucleation treatment. The disagreement for the data at $V_b = -20$ V may be attributed to some inhomogenity of the deposit after the nucleation treatment, caused by a small drift of ion energy in the vicinity of the threshold for shallow ion implantation, as described later. The nucleation density at $V_b = 0$ V is as low as that without any pretreatment. However, it shows a large increase by three orders of magnitude with increasing V_b from 0 to −50 V, then decreases drastically for V_b above −50 V. The maximum nucleation density, $\sim 10^8$ cm^{-2} at $V_b = -50$ V, is higher than $\sim 10^7$ cm^{-2} obtained with the conventional scratching pretreatment using diamond powder. The threshold V_b for the onset of nucleation enhancement lies between −20 and −30 V with a narrow V_b window (20–30 V) for the nucleation enhancement. The variation of nucleation density with ion energy has also been shown in a similar low-pressure study by plasma-beam deposition, where the density was maximized for ion energies close to 100 eV.[9]

Raman spectra for the deposits after the nucleation treatment are shown in Fig. 4(a). The deposits only exhibited the broad *D* and *G* line peaks at around 1350 and 1580–1600 cm^{-1}, originating from amorphous graphitic carbon, without showing a diamond peak. This is because the crystallite sizes were too small to be detected, due to enhanced phonon scattering from the boundaries of the Brillouin zone,[17] and/or a small cross section of diamond for visible Raman scattering by a factor of one-sixtieth relative to graphitic carbon.[18] To further examine the Raman spectra in Fig. 4(a), the FWHM of the *G* line peak and the ratio of the *D* peak to the *G* peak intensities (I_D/I_G) are plotted in

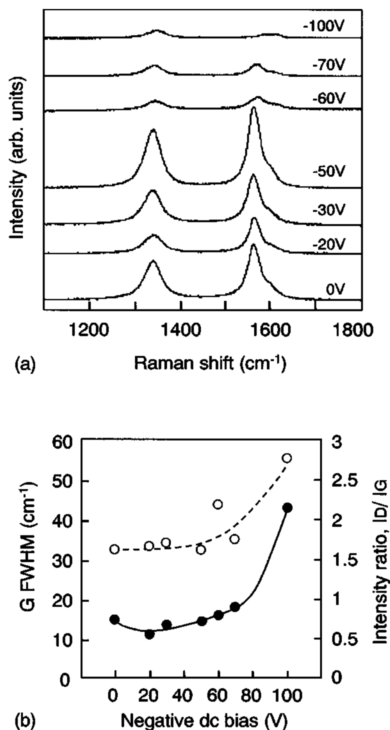

FIG. 4. Raman spectra for the deposits after the nucleation treatment with various substrate bias voltages. (b) G peak FWHM (open circles) and ratio of the D peak to G peak intensities (filled circles). The solid and dashed curves in (b) are guides to the eyes.

Fig. 4(b) as a function of V_b. The trends in the G peak FWHM and the I_D/I_G ratio for the change in V_b are very similar. They show minimum for V_b between 0 and -50 V, gently increase for V_b exceeding -50 V, and drastically increase at $V_b=-100$ V. An increase in G peak FWHM has been ascribed to an increase in sp^2 bond angle disorder of trivalent carbon atoms in a honeycomb network, while an increase in I_D/I_G ratio is correlated to a decrease in the average in-plane size of graphitic sp^2 domains.[19] According to these relations, the following hypothesis can be obtained with respect to the structure of carbon sp^2 phase. For low V_b (0 to -50 V), the sp^2 bond angle disorder was small and the size of sp^2 domains was large. For high V_b (-50–-100 V), an increasing ion-bombardment energy increased the amount and/or degree of sp^2 bond angle disorder and enhanced the bond breaking of sp^2 domains toward small domain sizes.

XRD patterns for the deposits after the nucleation treatment are shown in Fig. 5. The diffraction patterns for V_b except -30 and -50 V have no definite features of diamond other than reflections from underlying Si substrates. The diffraction patterns for $V_b=-30$ and -50 V show reflections peaked at 43.7° and 43.4°, respectively, both of which are assigned exclusively to the {111} planes of cubic diamond normally observed at 43.9° and partly to the {101} planes of graphite normally at 44.6°. The possibility of the {100} planes of lonsdaleite normally at 43.9° is precluded because a concomitant reflection from the primary {002} planes normally at 41.2° is absent. The relatively low intensity of diamond {111} planes could presumably be due to small crystallite sizes and/or highly defective structures. The other diamond features such as {220} and {311} planes normally at 75.7° and 91.2° are not observed. The results strongly indicate that diamond grains with low crystallinity are embedded in a matrix of amorphous graphitic carbon.

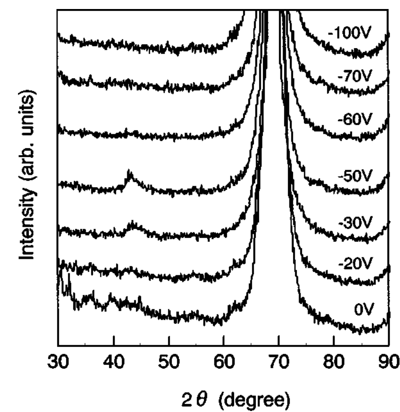

FIG. 5. XRD patterns for the deposits after the nucleation treatment with various substrate bias voltages.

Cross-sectional TEM bright-field images and SAED patterns for the deposits after the nucleation treatment for $V_b=-30$ V are shown in Figs. 6 and 7, respectively. In a low magnification image [Fig. 6(a)], an amorphous carbon film about 1 μm thick is seen to grow on the Si substrate. In a high magnification image near the interface between the Si and amorphous film [Fig. 6(b)], many small particles occasionally showing crystal lattice fringes are embedded in the amorphous carbon film. The particles are assigned to diamond and other carbonaceous phases like graphite. The particle sizes are mostly estimated to be 20–50 nm by measuring the size of dark domains. Furthermore, a SiC interlayer about 15 nm thick is grown just above the Si, and many SiC crystalline particles (dark domains) with sizes smaller than 20 nm are located almost parallel to the interface between the Si and SiC interlayer. It is important to note that there is a "blank" amorphous interlayer about 20 nm thick containing no particles between the amorphous film and the SiC interlayer. The SAED pattern in Fig. 7(a) for the Si and deposit shows some β-SiC diffraction spots just outside the Si diffraction spots, in addition to a faint diffraction ring from β-SiC. This means that a part of the SiC phase has a random orientation, but the rest has a preferred orientation with respect to the Si. In addition, a faint diffraction ring of diamond {111} planes can be observed (marked by a half-circular dashed line). The SAED pattern in Fig. 7(b) for the crystalline particle region in the amorphous carbon film clearly shows the rotational symmetry of the rings corresponding to the {111} and {220} planes of diamond. The broad intensity maximum for the diamond rings suggests small crystallite sizes and/or highly defective structures. The results indicate that diamond nuclei with random orientation were formed and then grown to a degree during the nucleation treatment.

The orientation between the SiC interlayer and Si substrate was further examined by cross-sectional high-resolution (HR) TEM. A HRTEM image of the SiC interlayer containing crystalline SiC particles (dark domains) corre-

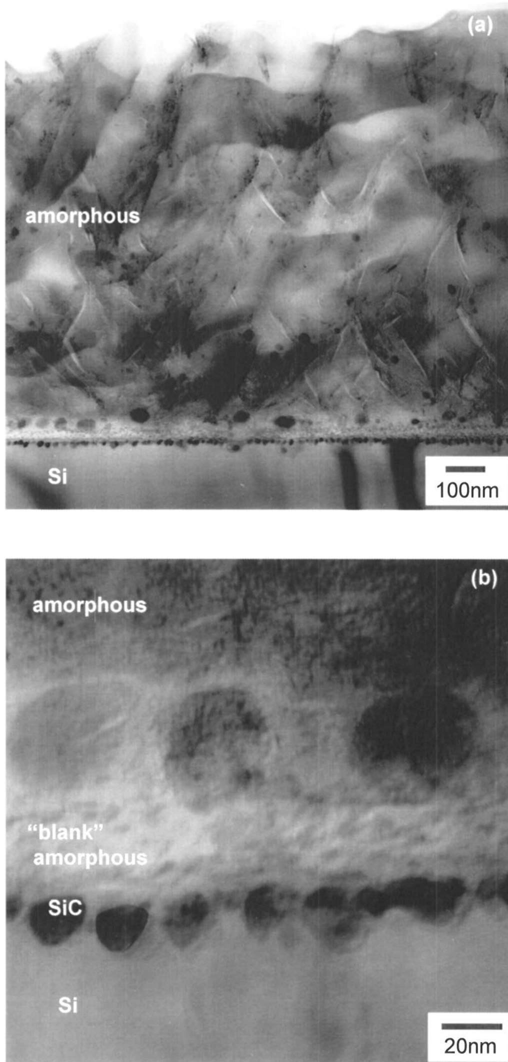

FIG. 6. Cross-sectional TEM images of the deposit after the nucleation treatment with $V_b = -30$ V; (a) whole view and (b) interfacial view.

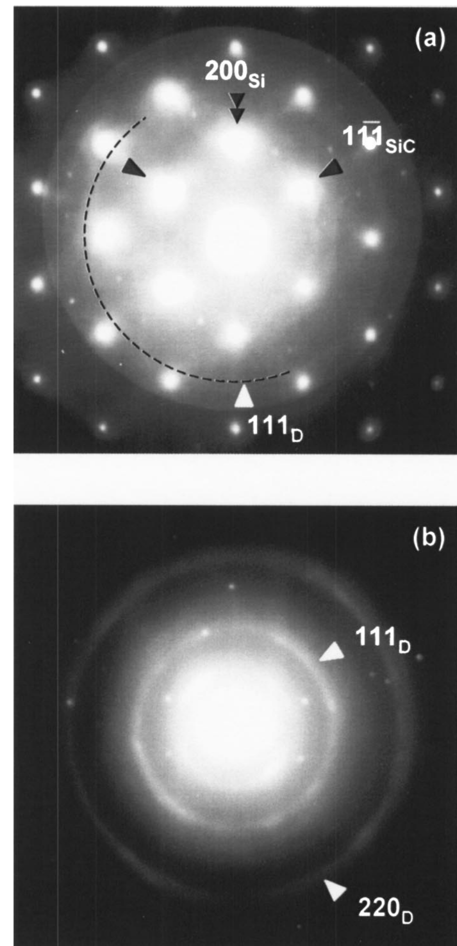

FIG. 7. SAED patterns of the deposit corresponding to Fig. 6 for (a) the deposit and the substrate, and (b) the crystalline region in the amorphous carbon film.

sponding to the sample in Figs. 6 and 7 is shown in Fig. 8(a). The lattice fringes of the {111} planes of β-SiC are nearly aligned to the {111} planes of Si with a misorientation angle of 10°. Unfortunately, a perfect exitaxy could not be observed so far. A HRTEM image of several small particles embedded in the amorphous carbon film is shown in Fig. 8(b). Small crystalline particles smaller than a few tens of nm with lattice fringes close to the lattice spacing of the {111} planes of diamond were occasionally observed, in agreement with the SAED results [Fig. 6(a) and 6(b)]. They were randomly oriented and highly defective. It should be noted that the particles with {111} crystal faces parallel to the incident electron direction can only be identified to be diamond by HRTEM. Therefore, the number density of diamond crystallites may actually be much higher than that observed in the HRTEM image. It is considered that the amorphous matrix was preferentially removed by etching and the diamond crystallites with relatively high crystallinity were enlarged to micron-sized crystals by subsequent growth under a normal deposition condition.

IV. DISCUSSION

Penetration of ions into a subsurface of a film (several atomic monolayers below a surface) occurs when the ion-bombardment energy exceeds a certain threshold (E_p):

$$E_p = E_d - E_b, \tag{2}$$

where E_d and E_b are the displacement energy of constituent atoms and the surface binding energy, respectively. For amorphous carbon films, theoretical values of E_p in the range of 20–30 eV are in good agreement with experimental ones.[20,21] For ion energies below E_p, the ions can only stick to a surface. Diamond nucleation proceeds on a surface via normal chemical processes of neutral radicals such as adsorption, migration, and clustering. The ion energy as low as several eV can assist kinetic processes of adsorbed radicals mainly by increasing their mobilities and formation probabilities of clusters.[13,22] However, the ions do not play the principal role in the nucleation. For ion energies above E_p, the implanted carbonaceous ions can cause a metastable increase in local film density and produce dense sp^3-bonded phase, the so-called "subplantation."[12]. We believe that the ion energy for the onset of nucleation enhancement in the

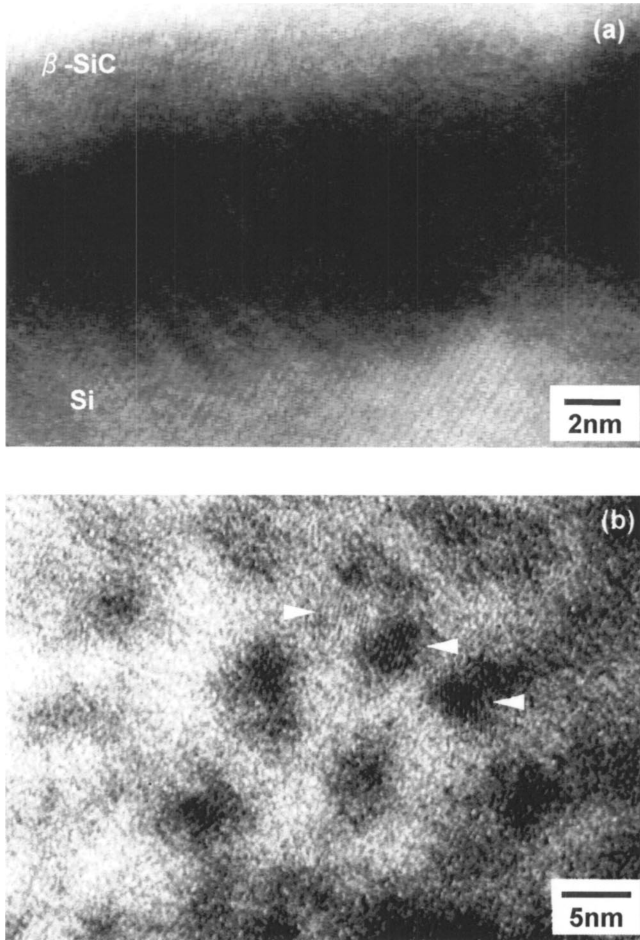

FIG. 8. HRTEM images of the deposit corresponding to Fig. 6, showing (a) a SiC interlayer nearly oriented to the Si substrate and (b) diamond crystallites embedded in the amorphous carbon film.

present experiments just corresponds to the beginning of this process. The excess energy of ions released by nuclear stopping will be dissipated as heat in a thermal spike. The optimum ion energy for a maximum sp^3 fraction is determined by a balance between an increase in sp^3 bonding by subplantation and a competitive increase in sp^2 bonding by thermally activated diffusion or damage-enhanced diffusion of atoms. A recent study suggested that this internal densification via physical processes is also applied to diamond nucleation.[23] According to this study, some of small diamond-like clusters among precipitated sp^3 clusters in a dense amorphous hydrogenated carbon (a-C:H) phase are grown to diamond nuclei through transformation of amorphous carbon to diamond at the amorphous-diamond interface by preferential atomic displacement. This process is highly promoted by implanted hydrogen ions. The diamond crystallites are thus embedded in a matrix of amorphous carbon, in accordance with our TEM observations.

The fractional increase in film density ($\Delta\rho/\rho$), associated with an increase in percentage of carbon sp^3 bonding, as a function of ion-bombardment energy (E_i) is expressed as[24]

$$\frac{\Delta\rho}{\rho}=\frac{f}{(R/J)-f+0.016p(E_i/E_0)^{5/3}}, \tag{3}$$

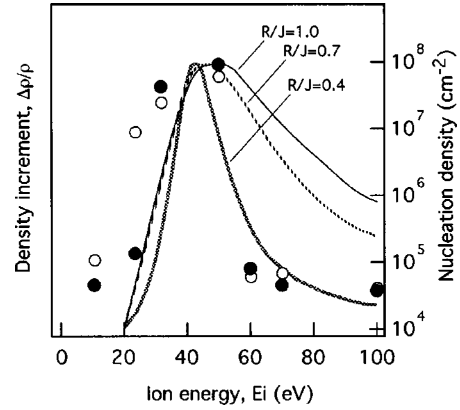

FIG. 9. Diamond nucleation density replotted from Fig. 3 [HFCVD (filled circles) and MW plasma CVD (open circles)] as a function of ion energy and normalized theoretical curves of Eq. (3) for $R/J=0.4$, 0.7, and 1.0.

where R is the depositing flux, J the ion flux, E_0 the activation energy of the density relaxation by thermal spike, and p a material-dependent parameter. f is the penetration probability of ions:

$$f=1-\exp\left(-\frac{E_i-E_p}{E_1}\right), \tag{4}$$

where E_1 is a spread parameter. By using the values of $E_0=1.5$ eV, $p=0.1$, and $E_1=16$ eV typical for a-C:H films[25] together with $E_p=20$ eV, $\Delta\rho/\rho$ can be obtained as functions of R/J and E_i. In Fig. 9, the nucleation density replotted as a function of E_i by taking V_{sh} for E_i is compared to the theoretical curves of Eq. (3) for $R/J=0.4$, 0.7, and 1.0. Each curve is normalized by its maximum to examine the trend against E_i. A reasonable fit to a rise in nucleation density for E_i from 23 to 50 eV is obtained with $R/J\approx1.0$. In contrast, a sharp decrease in nucleation density for E_i above 50 eV is described by the curves with smaller R/J. It should be noted that R/J varies with E_i, as expected from the Child-Langmuir law: $J\propto V_{sh}^{3/2}$. This indicates that R/J decreases with increasing E_i. Thus, the values of R/J are smaller than those in a-C:H deposition[25,26] and almost equal to those in c-BN deposition.[27] This is mainly because $T_s\sim700\,^\circ$C in the present experiments was much higher than $T_s\sim$room-temperature in a-C:H deposition, so that adsorbed neutral radicals should immediately desorb the surface, resulting in a minor contribution to R. In fact, at $V_b=-30$ V, the ratio of the net deposited carbon flux (4×10^{15} cm^{-2} s^{-1}) derived from the film growth rate by assuming a density of 2.8 gcm^{-3} to the ion current density (3 mA cm^{-2}) measured in an ECR H_2 plasma using a Langmuir probe was about 0.2. In spite of an underestimate due to the removed flux by etching, this alternate flux ratio seems to support the validity of R/J used in the calculation. Although the calculation may still include numerical errors in Eqs. (3) and (4), it enables us to understand how the nucleation density is enhanced at specific ion energies at least qualitatively. Figure 9 shows that the trend in the nucleation density is related with the density increment and hence the net increase in sp^3 fraction for the variations of R/J as well as E_i.

The preceding results confirm the ion-induced nucleation process beneath a surface, not the conventional one on a surface. Some of low-pressure studies using defined ion energies have demonstrated similar nucleation processes, where small diamond crystallites are embedded in a matrix of amorphous carbon film.[7–11] However, our ion energies (20–50 eV) for the nucleation enhancement are totally lower than their ion energies ($\sim$100–600 eV) presumably for two reasons. First, a high-density plasma with a high ion-to-neutral flux ratio tends to reduce R/J and shift an optimum ion-energy range to lower energies, as indicated by Eq. (3). Second, a high substrate temperature has been shown to reduce the critical radius of diamond,[28] corresponding to the energy barrier for the nucleation. This reduction facilitates diamond nucleation even at low ion energies and low efficiencies of atomic displacement since small diamond-like clusters can readily reach its small critical size. On the other hand, we could not observe any sign of diamond orientation, consistent with other low-pressure studies. This result is rather different from that in the BEN technique. The crystallites embedded in amorphous carbon films are randomly oriented, while those nucleated on Si steps can be oriented to the Si.[23]. If the nucleation pathway in the present study were broadly identical to the BEN, the orientation would be made possible by further optimizing the nucleation treatment.

V. CONCLUSION

The dependence of diamond nucleation density on ion-bombardment energy was systematically studied. A bare Si substrate was negatively biased to several tens of V in the ECR 50% $CH_4-50\%\,H_2$ plasma at 1 mTorr for the nucleation treatment, and then exposed to a typical HFCVD system at 40 Torr for growing the formed nuclei to large crystals. The nucleation density after the growth was enhanced up to $\sim 10^8$ cm^{-2} for V_b of -20 to -50 V and sharply decreased to $\sim 10^4$ cm^{-2} for V_b exceeding -50 V. Plasma potential measurement revealed that the threshold and optimum ion energies for the nucleation enhancement were 20–30 eV and around 50 eV, respectively, just above the threshold for shallow ion implantation. SEM and Raman spectroscopy revealed that the morphology and crystallinity of diamond as well as the nucleation density after the growth strongly depended on V_b used in the nucleation treatment. Cross-sectional TEM and SAED for the deposits after the nucleation treatment at an ion energy of around 30 eV demonstrated that diamond crystallites smaller than a few tens of nm with random orientation were embedded in a matrix of amorphous carbon. The interface structure was interpreted as, in the order of sequence, Si, SiC particles, SiC layer nearly oriented to the Si, amorphous carbon, and amorphous carbon containing diamond and nondiamond particles. The variation of nucleation density with ion energy was well described by the fractional increase in carbon sp^3 bonding, as the possible nucleation sites, based on the subplantation model.

ACKNOWLEDGMENTS

This research was conducted at the Institute for Ionized Gas and Laser Research at Kyushu University.

*Author to whom all correspondence should be addressed. Electronic address: teii@asem.kyushu-u.ac.jp

[1] *Handbook of Industrial Diamonds and Diamond Films*, M. A. Prelas, G. Popovici, and L. K. Bigelow (Dekker, New York, 1998).
[2] S. Yugo, T. Kanai, T. Kimura, and T. Muto, Appl. Phys. Lett. **58**, 1036 (1991).
[3] B.R. Stoner, G.-H.M. Ma, S.D. Wolter, and J.T. Glass, Phys. Rev. B **45**, 11067 (1992).
[4] J. Gerber, S. Sattel, H. Ehrhardt, J. Robertson, P. Wurzinger, and P. Pongratz, J. Appl. Phys. **79**, 4388 (1996).
[5] X. Jiang, W.J. Zhang, and C.-P. Klages, Phys. Rev. B **58**, 7064 (1998).
[6] K. Teii and T. Yoshida, J. Appl. Phys. **85**, 1864 (1999).
[7] T. Mōri and Y. Namba, J. Appl. Phys. **55**, 3276 (1985).
[8] S.R.P. Silva, S. Xu, B.X. Tay, H.S. Tan, and W.I. Milne, Appl. Phys. Lett. **69**, 491 (1996).
[9] S. Sattel, J. Robertson, M. Scheib, and H. Ehrhardt, Appl. Phys. Lett. **69**, 497 (1996).
[10] M. Zarrabian, N. Fouches-Coulon, G. Turban, C. Marhic, and M. Lancin, Appl. Phys. Lett. **70**, 2535 (1997).
[11] W.J. Zhang, X.S. Sun, H.Y. Peng, N. Wang, C.S. Lee, I. Bello, and S.T. Lee, Phys. Rev. B **61**, 5579 (2000).
[12] Y. Lifshitz, S.R. Kasi, and J.W. Rabalais, Phys. Rev. Lett. **62**, 1290 (1989).
[13] K. Teii, Appl. Phys. Lett. **74**, 4067 (1999); Phys. Rev. B **64**, 125327 (2001).
[14] H.W. Ellis, R.Y. Pai, E.W. McDaniel, E.A. Mason, and L.A. Viehland, Nucl. Data Tables **17**, 177 (1976).
[15] K. Teii, M. Hori, and T. Goto, J. Appl. Phys. **92**, 4103 (2002).
[16] Y. Kouzuma, K. Teii, K. Uchino, and K. Muraoka, Jpn. J. Appl. Phys., Part 1 **41**, 5749 (2002).
[17] M. Yoshikawa, Y. Mori, H. Obata, M. Maegawa, G. Katagiri, H. Ishida, and A. Ishitani, Appl. Phys. Lett. **67**, 694 (1995).
[18] N. Wada and S.A. Solin, Physica B **105**, 353 (1981).
[19] F. Tuinstra and J.L. Koenig, J. Chem. Phys. **53**, 1126 (1970).
[20] P.J. Fallon, V.S. Veerasamy, C.A. Davis, J. Robertson, G.A.J. Amaratunga, W.I. Milne, and J. Koskinen, Phys. Rev. B **48**, 4777 (1993).
[21] Y. Lifshitz, G.D. Lempert, and E. Grossman, Phys. Rev. Lett. **72**, 2753 (1994).
[22] K. Teii, M. Hori, and T. Goto, J. Appl. Phys. **89**, 4714 (2001).
[23] Y. Lifshitz, Th. Köhler, Th. Frauenheim, I. Guzmann, A. Hoffman, R.Q. Zhang, X.T. Zhou, and S.T. Lee, Science **297**, 1531 (2002).
[24] J. Robertson, Diamond Relat. Mater. **3**, 361 (1994).
[25] M. Weiler, S. Sattel, K. Jung, H. Ehrhardt, V.S. Veerasamy, and J. Robertson, Appl. Phys. Lett. **64**, 2797 (1994).
[26] R.G. Lacerda and F.C. Marques, Appl. Phys. Lett. **73**, 617 (1998).
[27] J. Robertson, Diamond Relat. Mater. **5**, 519 (1996).
[28] M.Y. Gamarnik, Nanostruct. Mater. **7**, 651 (1996).